Check for updates

Polymers for Advanced Technologies

WILEY

polymers for advanced technologies

RESEARCH ARTICLE OPEN ACCESS

Prediction and Optimization of PETG Part Hardness in 3D Printing: A Comparative Study of Experimental Design Methods

Osman Ulkir[1] | Arif Karadag[2]

[1]Department of Electric and Energy, Mus Alparslan University, Mus, Turkey | [2]Department of Motor Vehicles and Transportation Technologies, Mus Alparslan University, Mus, Turkey

Correspondence: Osman Ulkir (o.ulkir@alparslan.edu.tr)

Received: 5 March 2025 | **Revised:** 22 April 2025 | **Accepted:** 27 May 2025

Funding: The authors received no specific funding for this work.

Keywords: BBD | DSD | fused deposition modeling | hardness | PETG | Taguchi design

ABSTRACT

This study compared Box-Behnken Design (BBD), Definitive Screening Design (DSD), and Taguchi design methods to predict and optimize surface hardness in polyethylene terephthalate glycol (PETG) parts fabricated by fused deposition modeling (FDM). Critical printing factors including layer thickness (LT), infill density (ID), nozzle temperature (NT), and printing speed (PS) were analyzed to develop accurate prediction models while minimizing experimental runs. The comparative analysis revealed that all three methods provided reliable hardness predictions, with BBD showing superior accuracy (3.74% error), followed by DSD (4.25%) and Taguchi (4.84%). ID emerged as the most influential factor on surface hardness across all methods. BBD required 27 experimental runs, while DSD and Taguchi needed only 13 and 9 runs, respectively, demonstrating significant efficiency in experimental design. The optimal parameter combinations were validated through confirmation tests, achieving maximum hardness values of 62.47 Shore D (Taguchi), 57.16 Shore D (BBD), and 59.95 Shore D (DSD). These findings provide practical guidelines for industrial applications, enabling manufacturers to select the most suitable design method based on their specific requirements for accuracy versus experimental efficiency in PETG part production.

1 | Introduction

Additive manufacturing (AM) is a technology that creates a layer-by-layer structure to produce physical objects from digital models, and in this respect, it brings revolutionary innovations to manufacturing processes [1]. The flexibility offered by AM offers significant advantages over traditional manufacturing methods thanks to its ability to produce complex geometric shapes and customized products quickly and at low cost [2]. AM technology, which is frequently used in various sectors such as aviation, automotive, healthcare, and defense industries, can produce with a wide variety of materials such as metal and plastic [3–5]. PETG is among the materials commonly used in AM, mainly because of its durability and flexibility [6].

FDM, one of the leading AM techniques, is extensively utilized for its affordability, low processing temperatures, and compatibility with various materials [7, 8]. The FDM is ideal for producing durable and functional parts from polymer-based materials and is therefore a common choice for processing durable thermoplastics such as PETG [9]. PETG is known for its high impact strength, good chemical resistance, and flexibility, and ensures that mechanical properties such as hardness are evaluated as an important quality criterion in parts used in various applications

This is an open access article under the terms of the Creative Commons Attribution License, which permits use, distribution and reproduction in any medium, provided the original work is properly cited.

© 2025 The Author(s). *Polymers for Advanced Technologies* published by John Wiley & Sons Ltd.

[10, 11]. In this context, predicting and optimizing the basic mechanical properties such as hardness of PETG material during FDM production is of critical importance for industrial and functional applications. The hardness properties of parts fabricated with FDM are directly affected by the parameters used in the fabrication process [12]. These parameters include variables such as layer thickness (LT), printing speed (PS), infill density (ID), raster angle (RA) and nozzle temperature (NT). Optimizing hardness values requires careful control of these parameters. However, considering the effects of many parameters simultaneously can make the experimental process complex and costly [13]. Therefore, experimental design methods play a vital role in evaluating and optimizing the effects of the parameters used in FDM processes on mechanical properties such as hardness.

Experimental design methods are important tools used to obtain optimal hardness values [14]. Different experimental design methods such as Plackett-Burman design, Box-Behnken design (BBD), factorial design, central composite design, simplex centroid, definitive screening design (DSD) and Taguchi design methods determine the critical parameters of each process that need to be optimized and increase the efficiency of the process by reducing the number of experiments [15–17]. In this study, BBD, DSD, and Taguchi experimental design methods were preferred. BBD is recognized as an effective method, particularly for evaluating second-order interactions, and it enhances model accuracy while minimizing the number of experiments, thereby contributing to the achievement of maximum hardness through detailed analysis of parameter interactions [18]. In addition, DSD is a method developed to quickly and efficiently identify important parameters in experiments with many variables, determining the key factors influencing hardness measurements by accounting for both main effects and second-order interactions [19]. Taguchi design is another experimental design method that has found a wide application in quality engineering [20].

Hardness measurement requirements have gained importance with expanding application areas and increasing performance expectations. Hardness, which is especially critical for mechanical strength and wear resistance, plays a major role for parts operating under high loads or with precise tolerances [21]. As 3D printing technologies advance, analyzing the impact of printing parameters on hardness has become increasingly important, given that hardness is a critical indicator in both quality assurance and material evaluation. Numerous research studies have been conducted to investigate and address this issue through various control parameters [22, 23]. Veeman et al. used machine learning models such as linear regression, decision tree, random forest, and adaboost to optimize process parameters and estimate hardness [24]. Hardness measurements of test samples fabricated from ABS material by FDM were made with shore D durometer. Four parameters such as ID, LT, and RA were evaluated at three levels. The random forest model performs better than other models. Mohan et al. investigated the effects of FDM input parameters on ABS polymer parts in 15 experimental sets with BBD [25]. The parameters such as ID, LT, and bed temperature had significant effects on density, printing time, surface roughness, and microhardness. The accuracy of the regression equation for all obtained responses was tested by validation study. Borah et al. aimed to predict the Rockwell hardness of FDM printed PEEK components by statistical and machine learning techniques [26]. RSM, ANFIS, and RNN were used for hardness estimation, and by integrating the RNN model with PSO, a hardness value of 66.89 RHN was obtained under 80% ID, 0.1 mm LT, and 25 mm/s PS. Hsueh et al. investigated the effect of NT and ID changes on the mechanical properties of PLA material in 3D printing with FDM [27]. Increasing ID and NT improved tensile modulus, strength, elongation, and Shore hardness, while UV curing increased hardness and rigidity but decreased durability. The findings may benefit researchers aiming at sustainable material fabrication. Ajay Kumar et al. analyzed the mechanical strength of carbon fiber reinforced PETG thermoplastics and optimized the machine parameters [28]. Tensile, bending, and hardness tests were performed on samples fabricated according to ASTM standard; PS, ID, and LT were optimized with Taguchi. The effects of the factors on strength were statistically investigated with analysis of variance (ANOVA). The optimum values were determined as tensile strength 31.57 MPa, flexural strength 35.05 MPa, and hardness 67.00 BHN. Literature review shows that the hardness of parts fabricated by FDM is greatly affected by the process parameters. Various studies have been conducted to improve and monitor the hardness, but these studies have some limitations [29–31]. Some parameters such as NT, PS, and RA have been investigated less. Therefore, further research is required to determine the effects of different combinations of process parameters on hardness. This study will assess the performance of experimental design methods in predicting and optimizing the hardness of FDM parts, aiming to bridge existing gaps and offer insights into the effectiveness of these approaches.

In this study, experimental design methods such as BBD, DSD, and Taguchi were compared to evaluate the hardness properties of PETG materials fabricated by FDM. This comparison process was applied in terms of hardness prediction, accuracy, and optimization. The aim of the study is to determine the most appropriate parameter combination by analyzing the effect of each experimental design method on hardness values. In addition, the effect of the experimental designs used on the experimental costs and analysis time was also investigated. ANOVA was performed to observe the effect of printing parameters on hardness. In addition, regression analysis was applied to mathematically model the hardness values obtained from experimental measurements.

2 | Materials and Methods

2.1 | Material

Creality brand red PETG filament was used for the printing process. This filament has a diameter of 1.75 mm, which is a choice that complies with common standards for 3D printers. PETG has a density of around 1.27 g/cm^3 and is a preferred material in industrial applications because of its high impact resistance and thermal stability [32, 33]. PETG has a glass transition temperature of around 80°C and a melting temperature of up to 260°C, making it suitable for projects with high temperature resistance. PETG is also known for its low moisture absorption capacity, which reduces the effect of moisture on the filament during the printing process, resulting in more consistent and high-quality prints [34]. These features make

10991581, 2025, 6, Downloaded from https://onlinelibrary.wiley.com/doi/10.1002/pat.70230 by Turkey National Provision, Wiley Online Library on [10/11/2025]. See the Terms and Conditions (https://onlinelibrary.wiley.com/terms-and-conditions) on Wiley Online Library for rules of use; OA articles are governed by the applicable Creative Commons License

PETG suitable for applications in contact with food, while also expanding its use in medical and engineering applications [35, 36].

2.2 | 3D Fabrication Process

The FDM method, widely recognized as one of the most popular AM techniques, was employed in the fabrication of ASTM D638-type tensile samples for hardness testing. This method melts the thermoplastic material by heating it through a nozzle and then creates a 3D model by depositing this molten material layer by layer [7, 37]. The process begins with the creation of the model in computer-aided design (CAD) software. In accordance with ASTM standards, the sample is first designed in CAD software, adhering to the required size, geometry, and specifications. The technical drawings and dimensions of the test specimen are shown in Figure 1a. After the model is completed, it is exported in standard triangle language (STL) format; this format records the surface geometry with the triangulation method and defines the layered structure required for the 3D printer. In the next step, the STL file is loaded into slicing software and the model is divided into layers by determining the printer's LT, PS and NT settings. The slicing process creates G-code commands that determine the printer's movement paths. When the G-code file is sent to the printer, the FDM printer melts the material at the specified temperature following these instructions and deposits it layer by layer to create a sample that complies with ASTM standards. Some samples whose fabrication process has been completed are given in Figure 1b. A total of 49 samples were fabricated according to the determined experimental design process.

In this study, the Creality K1C 3D printer was used in the fabrication process (Figure 1c). This printer is a model that stands out with its features that can print at high speed and precision. With a maximum printing speed of 600 mm/s, this printer reaches a high melt output rate of 32 mm^3/s, allowing complex geometries to be fabricated in a short time. It also provides a stable printing environment in the production of ASTM D638 type tensile test specimens that require precision [38]. The printer's nozzle temperature can reach up to 300°C, and the printing platform can reach up to 100°C, which allows it to work with a wide range of materials.

Literature knowledge, researchers' previous studies, and experiments effectively determined fixed and variable parameters. The hardness of the samples produced with varying parameters such as LT, ID, NT, PS, and different levels of these parameters was measured. The levels of the selected process factors were determined based on the literature review and the existing FDM machine [39]. The printing factors used in the experimental design and their level values are shown in Table 1.

2.3 | Experimental Design

While determining the average hardness values, measurements were made considering the material processing direction of the fabricated sample. In determining the optimum values of FDM printing factors, an experimental design was made to minimize the time and cost factors that negatively affect the experimental process. The PETG hardness profile was

TABLE 1 | Printing factors with three levels used in the experiment.

Factors	Symbol	Units	Level 1	Level 2	Level 3
			−1	0	1
Layer thickness	LT	µm	100	200	300
Infill density	ID	mm	50	75	100
Nozzle temperature	NT	°C	240	250	260
Printing speed	PS	mm/s	60	90	120

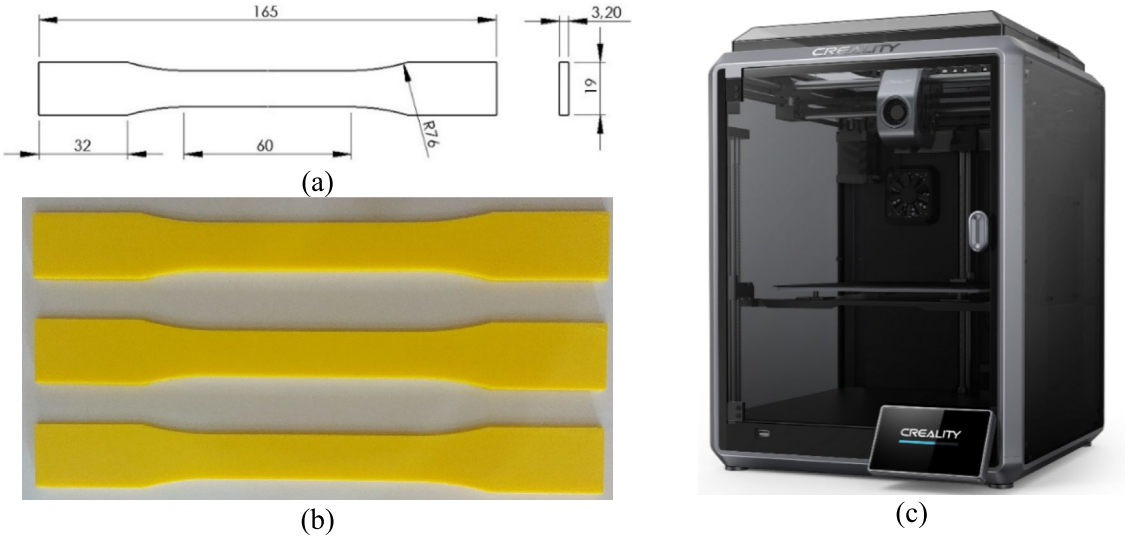

FIGURE 1 | (a) The specimen dimensions (mm). (b) Some test samples fabricated with a 3D printer. (c) Creality K1C 3D printer.

10991381, 2025, 6, Downloaded from https://onlinelibrary.wiley.com/doi/10.1002/pat.70230 by Turkey National Provision, Wiley Online Library on [10/11/2025]. See the Terms and Conditions (https://onlinelibrary.wiley.com/terms-and-conditions) on Wiley Online Library for rules of use; OA articles are governed by the applicable Creative Commons License

TABLE 2 | The average Shore D hardness obtained for BBD, DSD, Taguchi design.

	Box-Behnken design					Definitive screening design					Taguchi design				
No	**LT**	**ID**	**NT**	**PS**	**Hardness**	**LT**	**ID**	**NT**	**PS**	**Hardness**	**LT**	**ID**	**NT**	**PS**	**Hardness**
1	0	0	0	0	46.39	−1	0	−1	1	46.56	−1	−1	−1	−1	44.78
2	−1	0	0	−1	52.87	−1	−1	1	1	45.49	−1	0	0	0	50.68
3	0	0	0	0	46.39	0	0	0	0	46.39	−1	1	1	1	57.68
4	1	0	1	0	46.38	0	−1	−1	−1	40.75	0	−1	0	1	39.75
5	1	0	−1	0	42.41	−1	1	1	−1	62.47	0	0	1	−1	50.75
6	−1	−1	0	0	45.13	1	1	−1	−1	48.93	0	1	−1	0	49.37
7	0	−1	0	1	39.75	1	−1	−1	1	36.02	1	−1	1	0	41.19
8	0	1	0	−1	54.08	−1	1	−1	0	53.65	1	0	−1	1	40.91
9	0	1	1	0	54.76	1	0	1	−1	48.35	1	1	0	−1	51.49
10	−1	0	1	0	53.15	0	1	1	1	52.69					
11	1	0	0	1	42.92	1	1	0	1	47.53					
12	0	0	−1	−1	45.62	1	−1	1	0	41.19					
13	1	−1	0	0	39.25	−1	−1	0	−1	46.94					
14	1	0	0	−1	46.12										
15	1	1	0	0	49.37										
16	−1	0	−1	0	48.15										
17	0	1	−1	0	49.37										
18	0	1	0	1	49.92										
19	0	0	0	0	46.39										
20	0	−1	0	−1	42.17										
21	0	−1	1	0	43.47										
22	0	0	−1	1	42.15										
23	−1	0	0	1	48.72										
24	0	0	1	−1	50.75										
25	0	0	1	1	46.92										
26	0	−1	−1	0	39.27										
27	−1	1	0	0	56.21										

determined by taking measurements at five different points from the top and bottom surfaces of the sample. ANOVA and regression analyses were applied to define and model the relationship between the surface hardness obtained from the experimental measurements and the printing parameters. Since the aim of the current study is to create prediction and optimization models, three experimental design methods were used. These are BBD, DSD, and Taguchi. These design methods provide great benefits by reducing the number of experiments. For example, the current study has four factors and three levels of parameters; therefore, 243 experimental runs are needed. However, the BBD, DSD, and Taguchi methods require only 27, 13, and 9 experimental runs, respectively (Table 2). Therefore, these designs have high prediction efficiency with less standard error and high precision.

2.4 | Measurement of Hardness

The hardness measurement of PETG tensile test samples fabricated with the FDM was performed using the TRONIC PD-801 Analog Shoremeter device, which can measure hardness on the Shore D scale. This device is suitable for the hardness measurement of many materials such as hard plastics, synthetic materials, and thermoplastics. First, a tensile test sample fabricated in accordance with ASTM standards was used for the hardness measurement. The hardness profile of the PETG material is determined by taking measurements at five different points from the top and bottom surfaces of the sample. The values obtained from each measurement give a general idea about the surface hardness of the sample. The general hardness value of the sample was calculated by taking the average of the measurements

10991581, 2025, 6, Downloaded from https://onlinelibrary.wiley.com/doi/10.1002/pat.70230 by Turkey National Provision, Wiley Online Library on [10/11/2025]. See the Terms and Conditions (https://onlinelibrary.wiley.com/terms-and-conditions) on Wiley Online Library for rules of use; OA articles are governed by the applicable Creative Commons License

taken on the top and bottom surfaces (Table 2). The results obtained in this way are used to understand the mechanical properties of the PETG sample fabricated with the FDM, and taking measurements from multiple points to ensure the repeatability of the test increases the reliability of the measurements.

2.5 | Box-Behnken Design

The BBD is a frequently preferred response surface methodology (RSM) approach among statistical experimental design and optimization methods. This method was developed specifically to determine the binary interactions and second-order effects of factors [40]. BBD requires fewer experiments than full factorial designs and provides both an economic and practical advantage by addressing high-level combinations of factors. Because of these characteristics, it is preferred in situations where process parameters must be optimized with limited resources or when experiments need to be conducted in a faster and more cost-effective manner [41]. When BBD is utilized to analyze the influence of three variables, like LT, NT, and PS, in a 3D printing process, the overall number of experimental runs can be substantially minimized.

Figure 2 describes the BBD in a three-factor system. Factor levels are usually selected at low, medium, and high values (e.g., −1, 0 and +1), but the experimental points are not at the highest or lowest levels of all factors [42]. The three axes in the plot represent each factor, and the levels on these axes indicate different values of the factors. BBD reduces the number of experiments by selecting points located in the middle of the edges and in the center, making it easier to understand the interactions between the factors. This increases the safety of the experiment and reduces the risks that may arise from extreme conditions in critical processes. In addition, BBD examines each factor at three levels, making it possible to effectively capture nonlinear effects and interactions between parameters [43].

2.6 | Definitive Screening Design

The DSD is an advanced experimental design method used to determine important factors in systems with a high number of factors and to optimize the process [44]. This design was developed to reveal the linear and quadratic effects of factors with a smaller number of experiments compared to other screening designs. It is especially preferred in cases where there are many factors, and the number of experiments needs to be minimized. One of the most striking features of DSD is that a single series of experiments can be used to both screen important factors and model their quadratic effects. Therefore, DSD is generally ideal for quickly determining which parameters are most important in the early stages of processes. These features make DSD attractive, especially in projects with limited resources or time frames [45]. In addition, it also offers flexibility, such as the addition of center points to verify the effects of certain factors in the experimental design process. Therefore, the high-throughput structure of DSD offers a fast, reliable, and cost-effective option for determining important factors in processes.

Figure 3 shows the basic structure of the DSD method. This method is used to outline the effects of a large number of factors, and each factor is analyzed at three levels (−1, 0, +1) [46]. In the plot, the experimental points are arranged in a certain balance, so that the main effects of the factors and their interactions can be more clearly separated. The middle points (level 0) allow the main effects to be examined independently and the nonlinear effects to be observed.

2.7 | Taguchi Design

The Taguchi is an experimental design method developed to improve quality and efficiency and used to understand and optimize the effects of factors on the results of a process [47]. This method is especially preferred for the goals of improving quality and reducing costs in production processes. The Taguchi analyzes both the main effects and interactions of factors and plans experiments to ensure that the system is least affected by external effects. The basic approach of this method is to provide quality not in costly control stages but in the design stage and to minimize variations that are the source of quality problems [48].

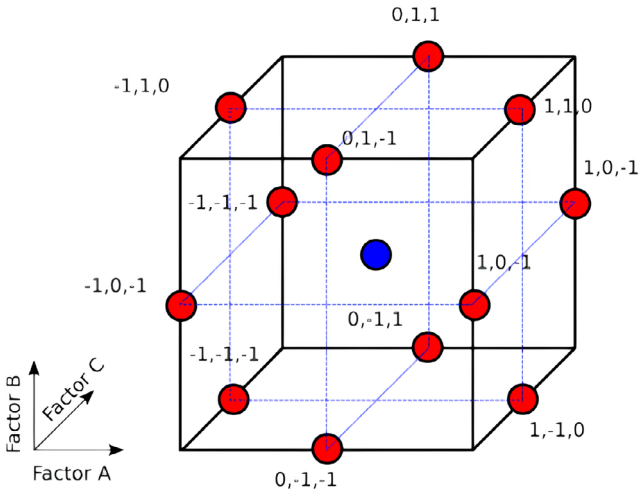

FIGURE 2 | Box-Behnken design methodology.

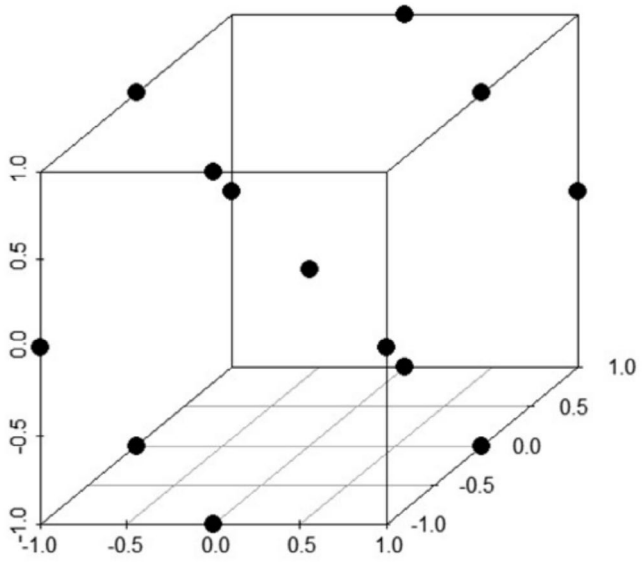

FIGURE 3 | Definitive screening design methodology.

10991581, 2025, 6, Downloaded from https://onlinelibrary.wiley.com/doi/10.1002/pat.70230 by Turkey National Provision, Wiley Online Library on [10/11/2025]. See the Terms and Conditions (https://onlinelibrary.wiley.com/terms-and-conditions) on Wiley Online Library for rules of use; OA articles are governed by the applicable Creative Commons License

Taguchi reduces the number of experiments by using orthogonal arrays in experimental design and thus minimizes cost and time. Taguchi also offers the advantage of minimizing variations in the process by calculating the Signal-to-Noise (S/N) ratio. This ratio shows how stable the performance in each experimental condition is against noise factors and is used as a quality metric that needs to be optimized [49]. In the Taguchi approach, the response variable is formulated as a function, and the robustness of the process is assessed by analyzing the S/N ratio.

$$S/N = -10\log\left(\frac{1}{n}\sum_{i=1}^{n}\frac{1}{y_i^2}\right) \quad (1)$$

Here, y_i is the response value in each experiment result and n is the total number of experiments. The S/N ratio obtained in this equation shows how little the process is affected by external factors. The Taguchi determines the optimum levels of process parameters using this mathematical approach and ensures that the output is closest to the desired quality characteristics.

2.8 | Optimization Methodology

The desirability function approach is employed to optimize the hardness of the samples, aiming to achieve the highest possible hardness values. A maximization-oriented desirability function is utilized to transform the hardness data into a normalized scale between 0 and 1, where values approaching 1 correspond to optimal hardness outcomes. This optimization method allows for the effective tuning of process parameters to maximize hardness, as outlined in Equation (2) below:

$$d = \begin{cases} 0 & if\, y \le L \\ \left(\frac{y-L}{U-L}\right)^r & if\, L < y < U \\ 1 & if\, y \ge U \end{cases} \quad (2)$$

where, d is the desirability value response at the experimental run, y is optimized response variable (hardness value), L is minimum acceptable value of the response variable, U is maximum desired limit value of the response variable, and r is slope parameter of the desirability function.

3 | Results and Discussion

3.1 | Main Effect and Surface Plots

In this section, graphical results of the methods used in the experimental design process are given. The relationship between the printing factors and hardness are examined using main effect plots based on Taguchi, as shown in Figure 4. In the Taguchi design, the experimental design was performed using the Taguchi L9 orthogonal array. A total of 9 experiments were conducted for this method. In the experimental design, the S/N ratio was used to optimize the determined parameters, ensure stability and ensure minimum process variability. The "larger is better" approach was used to determine the highest average

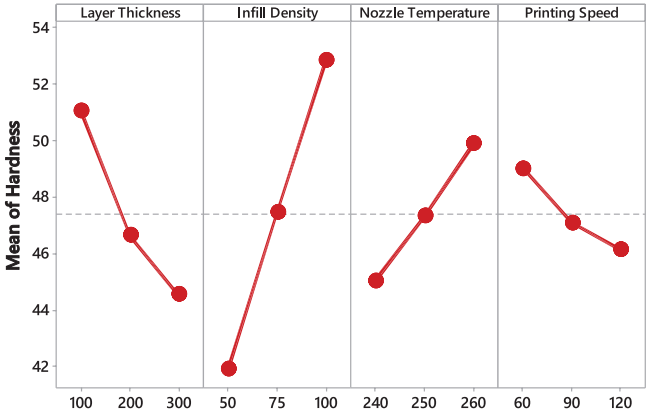

FIGURE 4 | Main effects of the 3D printed parts.

hardness values. The average hardness values and the corresponding values for each printing factor are given in Table 2. The average of five surface hardness measurements were taken to obtain these results. These measurements ranged from 39.75 to 57.68.

The optimum levels of the printing factors are at the highest point of the relevant level according to the graph. Therefore, the best result is obtained at the levels of LT, ID, NT, and PS parameters of 100 μm, 100%, 260°C, and 60 mm/s, respectively. As a result, the best average hardness value among the experiments was obtained in experiment number 3 with "100 μm" LT, "%100" ID, "260°C" NT, and "120 mm/s" PS. The hardness value can be controlled by the printing parameters (Figure 4). The ID parameter is the most important in terms of hardness value. Increasing the ID in the samples increases the hardness value. As the ID of the parts increases, the internal structure becomes tighter, and the material density increases. This increases structural durability and causes the hardness to increase. Although the effect of the NT parameter is slightly lower, hard parts can be obtained at high temperatures. As the NT increases, a better bond is achieved between the material layers, which creates a more robust structure and increases hardness. The hardness value deteriorates as the PS increases. As the PS increases, it becomes difficult for the layers to settle properly and merge sufficiently, which creates gaps in the internal structure and leads to a decrease in hardness. The hardness of the parts decreases as the LT parameter increases. As the LT increases, the bonding force between the layers decreases and the bond between the layers weakens; this leaves gaps in the internal structure of the part, causing the hardness to decrease.

The BBD experiments and results of the design are given in Table 2. A total of 27 experiments were performed. The hardness measurement results are between 39.25 and 56.21. The results from the analysis are shown as a surface plot (Figure 5). Thus, the interaction between the printing factors and their effects on hardness was observed. Among the experiments, the best average hardness value was obtained in experiment number 27 with "100 μm" LT, "100%" ID, "250°C" NT, and "90 mm/s" PS.

In Figure 5a, the relationship between hardness, ID, and LT is shown in 3D. The surface slope in the graph shows that ID has a positive effect on hardness and LT has a negative effect.

10991581, 2025, 6, Downloaded from https://onlinelibrary.wiley.com/doi/10.1002/pat.70230 by Turkey National Provision, Wiley Online Library on [10/11/2025]. See the Terms and Conditions (https://onlinelibrary.wiley.com/terms-and-conditions) on Wiley Online Library for rules of use; OA articles are governed by the applicable Creative Commons License

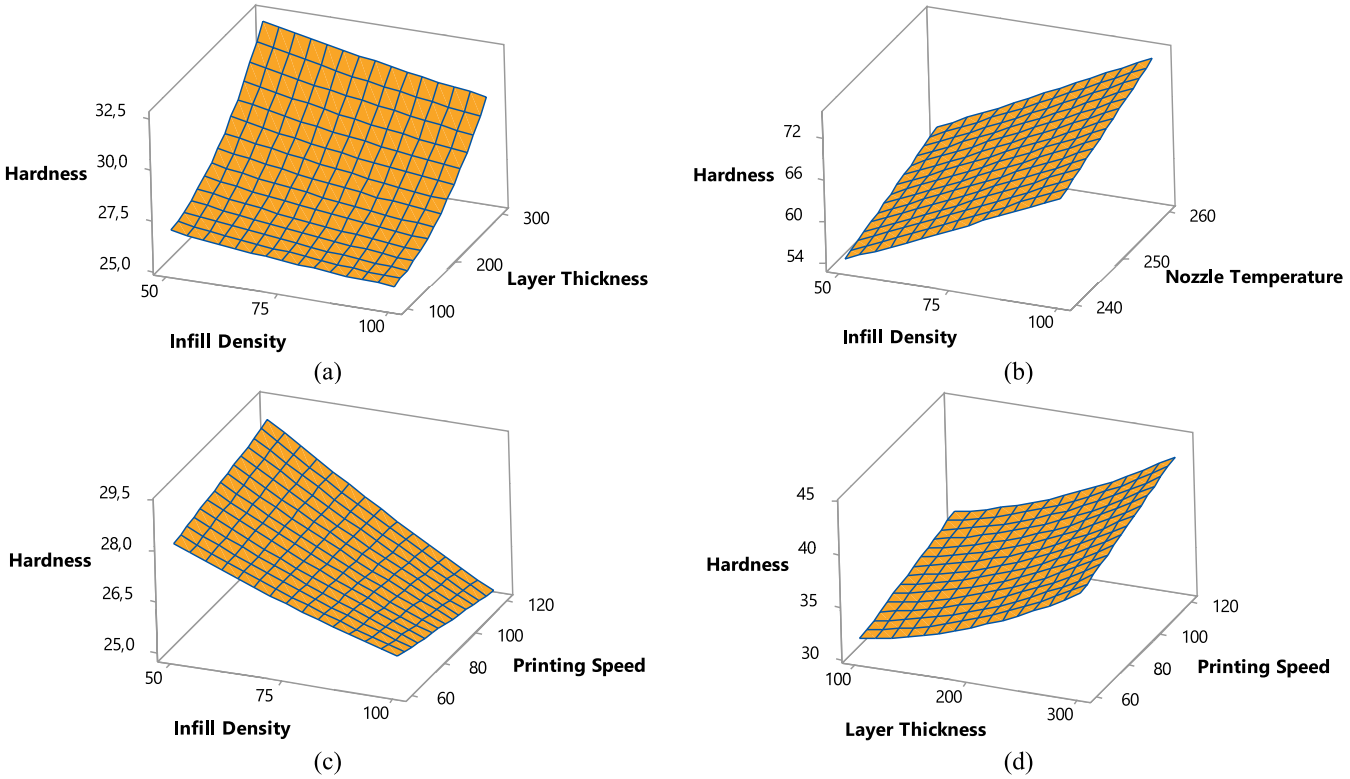

FIGURE 5 | Surface plots of Box-Behnken design results.

Therefore, the highest hardness value is obtained when the ID is high and LT is low. The surface slope of the graph in Figure 5b shows that ID and NT have a positive effect on hardness, i.e., increasing both parameters increases the hardness. The highest hardness value is obtained when the ID and NT are high. The surface slope of the graph in Figure 5c shows that ID has a positive effect on hardness and PS has a negative effect. The highest hardness is obtained when the ID is high and PS is low. Figure 5d shows that LT and PS have a negative effect on hardness, i.e., increasing both parameters decreases the hardness. As a result, the ID parameter among the printing factors has a great effect on hardness. High hardness parts can be obtained by choosing low LT and PS together with high ID and NT.

The DSD experiments and results of the design are given in Table 2. A total of 13 experiments were conducted. Hardness measurement results are between 36.02 and 62.47. The results of the analysis are shown as a contour plot (Figure 6). Thus, the interaction between the printing factors and their effects on surface hardness was observed. The highest effect is in the ID factor. The best average hardness value was obtained in experiment number 5 with "100 μm" LT, "100%" ID, "260°C" NT, and "60 mm/s" PS.

Similar results to other design methods can be seen from the graphs in Figure 6. ID is an important factor that can affect hardness properties. Figure 6a shows the relationship between NT and ID. In general, an increase in hardness values is observed as ID and NT increase. This shows that ID and NT can positively affect material properties. Higher temperatures and densities result in harder part production. As NT increases, higher hardness values are generally obtained (Figure 6b). Especially around 255°C, hardness values show a more significant increase when combined with lower LT. As thicker layers are used, a significant decrease in hardness is observed after a certain point. Especially when the NT exceeds 250°C, it is a factor that increases hardness. Figure 6c shows the effect of NT and PS on part hardness. The hardness values generally increase as the NT increases. Especially at temperatures of 250°C and above, a significant increase is observed in the hardness values. As the PS increases, the hardness generally tends to decrease. Lower hardness values can be obtained especially in high-speed printing. Finally, the relationship between ID and LT was observed (Figure 6c). The graph generally shows that the hardness values increase as the ID increases. The hardness obtained is higher when high ID and thin layers are used. Hardness values tend to rise in cases where the ID is 80% or above, demonstrating its significant effect on material strength.

3.2 | Analysis of Variance

ANOVA was applied to determine whether the printing factor settings caused a significant change in surface hardness and which parameters were most effective. This analysis was performed at a 95% confidence interval for all experimental designs. The ANOVA results of the experiments performed with the Taguchi are given in Table 3. The ANOVA table summarizes the statistical outcomes of the variance analysis and indicates which factors significantly influence the dependent variable. The *F* and *P* values were used to verify the significance of the parameters. The *F* value is a statistic that tests whether the effect of a factor on the dependent variable is significant in the ANOVA. The *F* value is calculated by dividing the mean square value of

10991381, 2025, 6, Downloaded from https://onlinelibrary.wiley.com/doi/10.1002/pat.70230 by Turkey National Provision, Wiley Online Library on [10/11/2025]. See the Terms and Conditions (https://onlinelibrary.wiley.com/terms-and-conditions) on Wiley Online Library for rules of use; OA articles are governed by the applicable Creative Commons License

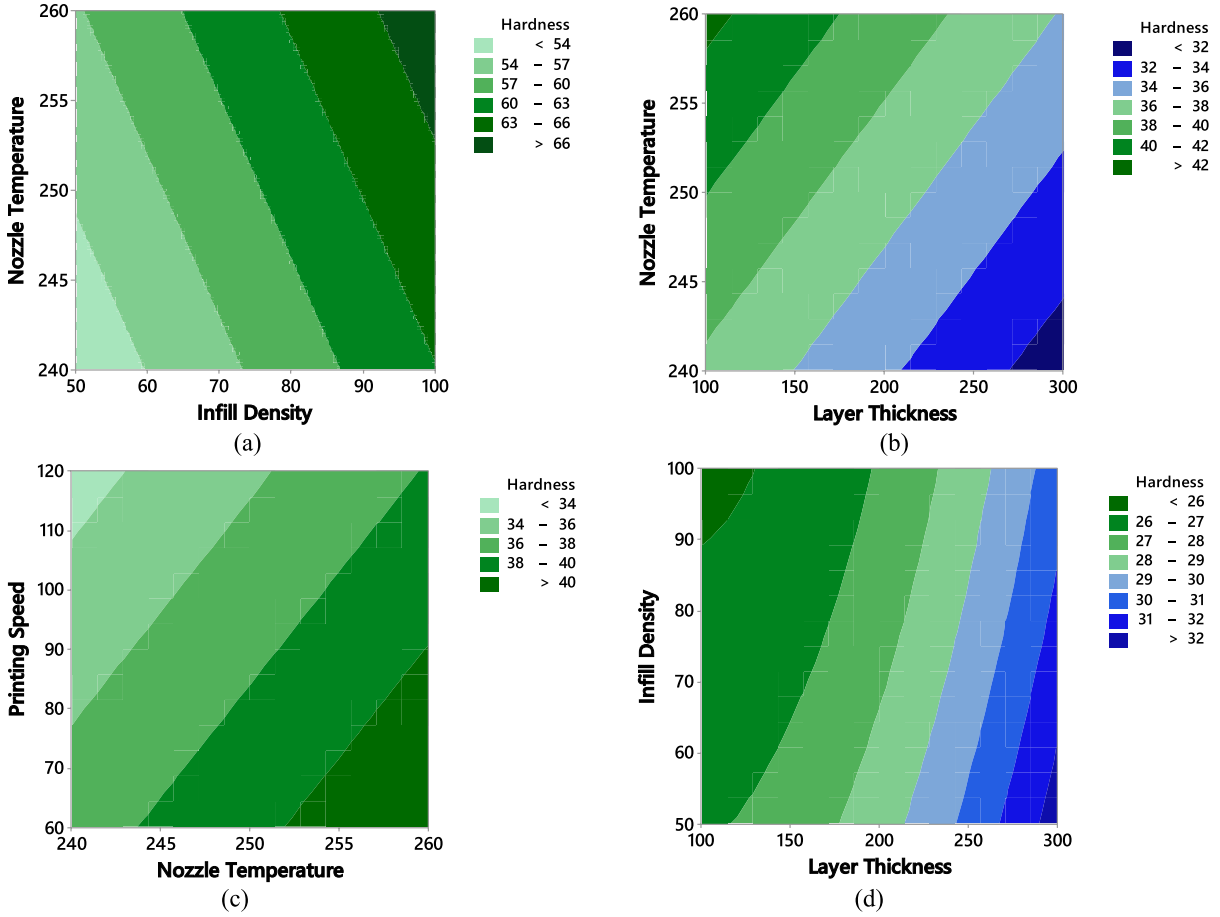

FIGURE 6 | Contour plots of definitive screening design results.

TABLE 3 | ANOVA results for Taguchi design.

Factor	DF	Adj SS	Adj MS	*F* value	*p*	Contribution (%)
Layer thickness	2	66.413	33.207	325.71	0.000	21.85
Infill density	2	179.54	89.768	951.38	0.000	**58.73**
Nozzle temperature	2	35.375	17.686	124.34	0.000	10.28
Printing speed	2	13.021	6.509	91.48	0.000	8.76
Error	4	0.127	0.267			0.38
Total	12	294.386				100

a factor by the mean square value. A high *F* value indicates that the effect of the factor on the dependent variable is greater than the error and therefore this effect is significant rather than coincidental. If the *F* value exceeds a certain threshold, then the factor is considered to create a significant difference between the groups and is supported by the *p* value; this indicates that the effects are statistically significant when $p < 0.05$.

The *p*-values in Table 3 indicate that all selected printing factors play an important and significant role in determining hardness. However, the effect values are quite different because of the different *F* values. The percentage impact rates of LT, ID, NT, and PS factors on hardness were found to be 21.85%, 58.73%, 10.28%, and 8.76%, respectively. The error rate for the average hardness was 0.38%. As a result, the factor with the highest effect on hardness was ID with a contribution rate of 58.73%. The lowest contribution was in the PS factor with 8.76%.

The ANOVA results of the experiments performed with the BBD are given in Table 4. The results indicate that the *p* values of all parameters remain within statistically significant limits, confirming their influence on the response variable. The percentage impact rates of LT, ID, NT, and PS factors on hardness were found to be 21.67%, 60.21%, 9.64%, and 7.56%, respectively. Like the Taguchi method, ID was the most influential parameter, accounting for 60.21% of the total effect. However, the

10991581, 2025, 6, Downloaded from https://onlinelibrary.wiley.com/doi/10.1002/pat.70230 by Turkey National Provision, Wiley Online Library on [10/11/2025]. See the Terms and Conditions (https://onlinelibrary.wiley.com/terms-and-conditions) on Wiley Online Library for rules of use; OA articles are governed by the applicable Creative Commons License

TABLE 4 | ANOVA results for Box-Behnken design.

Factor	DF	Adj SS	Adj MS	*F* value	*p*	Contribution (%)
Layer thickness	2	125.422	62.711	456.13	0.000	21.67
Infill density	2	348.583	174.291	1267.73	0.000	**60.21**
Nozzle temperature	2	67.522	33.761	245.56	0.000	9.64
Printing speed	2	37.561	18.781	136.61	0.000	7.56
Error	8	2.475	0.137			0.92
Total	16	581.563				100

TABLE 5 | ANOVA results for definitive screening design.

Factor	DF	Adj SS	Adj MS	*F* value	*p*	Contribution (%)
Layer thickness	2	111.590	55.795	42.92	0.001	21.65
Infill density	2	301.307	150.564	115.88	0.000	**58.42**
Nozzle temperature	2	59.417	29.708	22.85	0.006	10.71
Printing speed	2	36.838	18.419	14.17	0.015	7.26
Error	12	5.201	1.30			1.96
Total	20	512.244	195			

error in the BBD was 0.92%, which was higher than that of the Taguchi.

The ANOVA results of the experiments performed with DSD are given in Table 5. Since the *p* values in the table are less than 0.05 for all parameters, they are significant. However, the significance of the LT, NT, and PS factors decreased compared to the other design methods. The percentage impact rates of LT, ID, NT, and PS factors on hardness were found to be 21.65%, 58.42%, 10.71%, and 7.26%, respectively. The error rate for the average hardness was 1.96%. The highest error value among the three design methods was calculated in the DSD. As in the other methods, the parameter with the highest impact was ID with 58.42%.

3.3 | Regression Model Results

Regression analysis was performed to numerically express the relationship between the printing factors and hardness. This analysis is a statistical technique used to examine the relationship between a dependent variable and one or more independent variables and to make predictions based on this relationship [50]. Researchers use regression analysis to understand how and to what extent variables affect each other, to determine the strength and direction of the relationships between them. This analysis allows for future predictions in the development of decision support systems, strategic planning, and various fields. In this study, real regression models were developed for hardness based on BBD, DSD, and Taguchi methods with a 95% confidence interval. The purpose of this model is to estimate the main effect, interaction effect, and second-order effect of printing factors on the average hardness. Equations (3–5) represent the regression models developed based on BBD, Taguchi, and DSD methods, respectively.

$$\begin{aligned} Hardness_{BBD} = {} & 30 - 0.09557\ Layer\ Thickness \\ & + 0.1890\ Infill\ Density \\ & + 0.058\ Nozzle\ Temperature \\ & - 0.0221\ Printing\ Speed \\ & - 0.000110\ Layer\ Thickness^2 \\ & + 0.000277 Infill\ Density^2 \\ & + 0.000087 Nozzle\ Temperature^2 \\ & - 0.000068 Printing\ Speed^2 \end{aligned} \tag{3}$$

$$\begin{aligned} Hardness_{Taguchi} = {} & 75 - 0.09918\ Layer\ Thickness \\ & + 0.2356\ Infill\ Density \\ & + 0.0557\ Nozzle\ Temperature \\ & - 0.0342\ Printing\ Speed \\ & - 0.000117\ Layer\ Thickness^2 \\ & + 0.000212 Infill\ Density^2 \\ & + 0.000094 Nozzle\ Temperature^2 \\ & - 0.0000833 Printing\ Speed^2 \end{aligned} \tag{4}$$

$$\begin{aligned} Hardness_{DSD} = {} & 276 - 0.0821\ Layer\ Thickness \\ & + 0.162\ Infill\ Density \\ & + 0.0413\ Nozzle\ Temperature \\ & - 0.0315\ Printing\ Speed \\ & - 0.000097\ Layer\ Thickness^2 \\ & + 0.00038 Infill\ Density^2 \\ & + 0.0000659 Nozzle\ Temperature^2 \\ & - 0.0000403 Printing\ Speed^2 \end{aligned} \tag{5}$$

10991381, 2025, 6, Downloaded from https://onlinelibrary.wiley.com/doi/10.1002/pat.70230 by Turkey National Provision, Wiley Online Library on [10/11/2025]. See the Terms and Conditions (https://onlinelibrary.wiley.com/terms-and-conditions) on Wiley Online Library for rules of use; OA articles are governed by the applicable Creative Commons License

In the regression models, positive coefficients indicate that the increase in the relevant model terms increases the hardness, while negative coefficients indicate that the increase in these terms decreases the surface hardness. For example, the positive coefficient value of infill density (0.189) indicates that the average value of hardness increases by 0.189 with a gradual increase in ID from a low level to a high level (Equation 3). The negative coefficient value of LT (0.09557) indicates that the average value of hardness decreases by 0.09557 with a gradual increase in LT from a low level to a high level. Equations (3–5) reveal that similar interpretations can be made for the remaining model terms as well. Additionally, Equation (3) shows that ID has a dominant effect on hardness, with a high coefficient value of 0.189, followed by other main effects, interaction terms, and quadratic effects such as LT (0.09557), NT (0.058), PS (0.0221), the quadratic term of ID (0.000277), and LT (0.00011). Similar insights apply to the other model terms presented in Equations (4) and (5).

Pareto chart was used to show the standardized effects of the factors on hardness. The standardized effects resulting from the application of the BBD are presented in Figure 7a. The graph shows the factors ranked from the largest to the smallest in terms of their effects on the hardness response variable. The red dashed line shows the significance level (2.08); the factors to the right of this line indicate that their effects on hardness are statistically significant. According to the graph, the factor with the strongest effect is **B** (ID). The effect of this factor on hardness is quite large and is clearly ahead of all other factors. ID is followed by **A** (LT), **C** (NT) and **D** (PS). In summary, this graph shows that the factor with the strongest effect on hardness is ID, followed by LT, NT, and PS, respectively. This information shows that ID is a parameter that should be paid special attention to in order to improve or optimize the hardness properties. The standardized effects obtained in the DSD method exhibited similar characteristics to BBD (Figure 7b). In this method, the most effective parameter was ID. Since the AA term (square effect of LT) in the DSD effect graph remains below the significance line, its effect on hardness is not statistically significant.

3.4 | Regression Model Adequacy

The accuracy and suitability of the regression models in Equations (3–5) were analyzed based on the residual plot, coefficient of determination (R^2), adjusted R^2 and estimated R^2. The regression analysis process was carried out at a confidence interval of 95%. The significance level of the analyses was tested through the p value. The normal residual plots and the predicted values using the results in Table 2 are shown in Figures 8–10. These results show that the p value of the test is less than 0.05 for all designs. The residuals fit the normal distribution, and the developed models are valid and suitable for predictions.

The residual plot results for the BBD are given in Figure 8. The hardness values measured for different experiments and predicted by the model are compared in Figure 8a. The predicted and actual values are quite close to each other and follow a similar trend. This shows that the model successfully predicts the hardness values and works with high accuracy. Figure 8b is a normal probability plot used to evaluate the normality of the residuals. In general, since most of the residuals are distributed close to the red line, the model largely fits the assumed normal distribution. This can be considered a positive sign of the accuracy and validity of the model, but deviations at the extreme points may indicate that there are deviations from the expected normality in a very small part of the model. In Figure 8c, the residuals are randomly distributed around the horizontal axis. The residuals do not show a trend up or down, indicating that there is no systematic error in the model and that the model largely satisfies the linear relationship assumption. However, the points appear to be slightly spread out, which may indicate that the model may make small errors in some predictions. From the zero line on the vertical axis, it is seen that some of the residuals go above this line and some fall below it (Figure 8d). This shows that the model fits well in some observations and falls short in some observations.

The residual plot results for the DSD are given in Figure 9. The actual and predicted values are generally close to each other (Figure 9a). This indicates that the model makes good predictions in most of the experiments. A positive linear relationship is generally observed from the results in Figure 9b, but it is understood that the model should be considered more carefully in some special cases. On the vertical axis, the residuals are generally distributed around zero as the predicted values increase (Figure 9c). However, the lack of a clear order or trend in the relationship for a few values may indicate that the model's

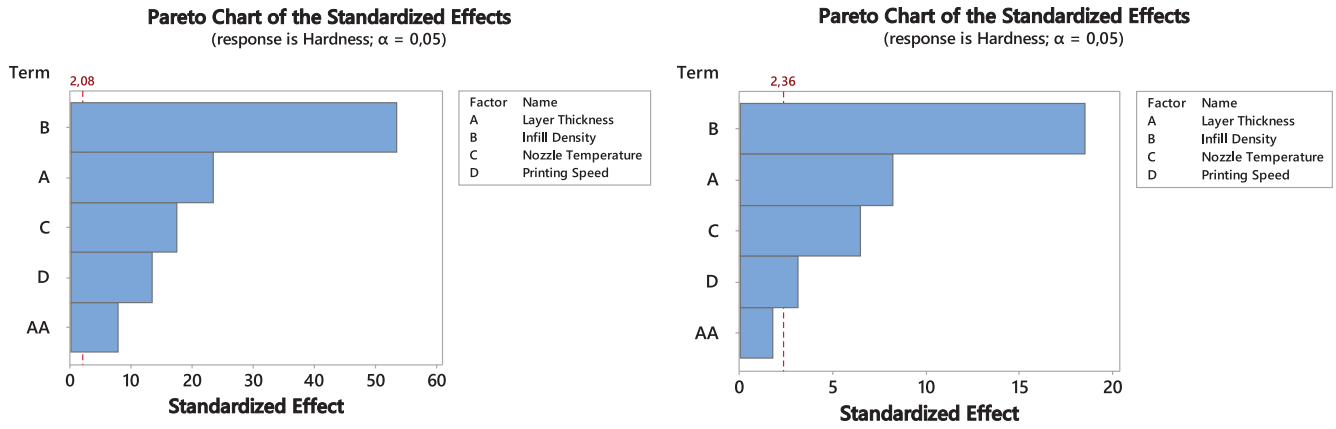

(a) BBD results (b) DSD results

FIGURE 7 | The pareto chart of the standardized effects for BBD and DSD.

10991581, 2025, 6, Downloaded from https://onlinelibrary.wiley.com/doi/10.1002/pat.70230 by Turkey National Provision, Wiley Online Library on [10/11/2025]. See the Terms and Conditions (https://onlinelibrary.wiley.com/terms-and-conditions) on Wiley Online Library for rules of use; OA articles are governed by the applicable Creative Commons License

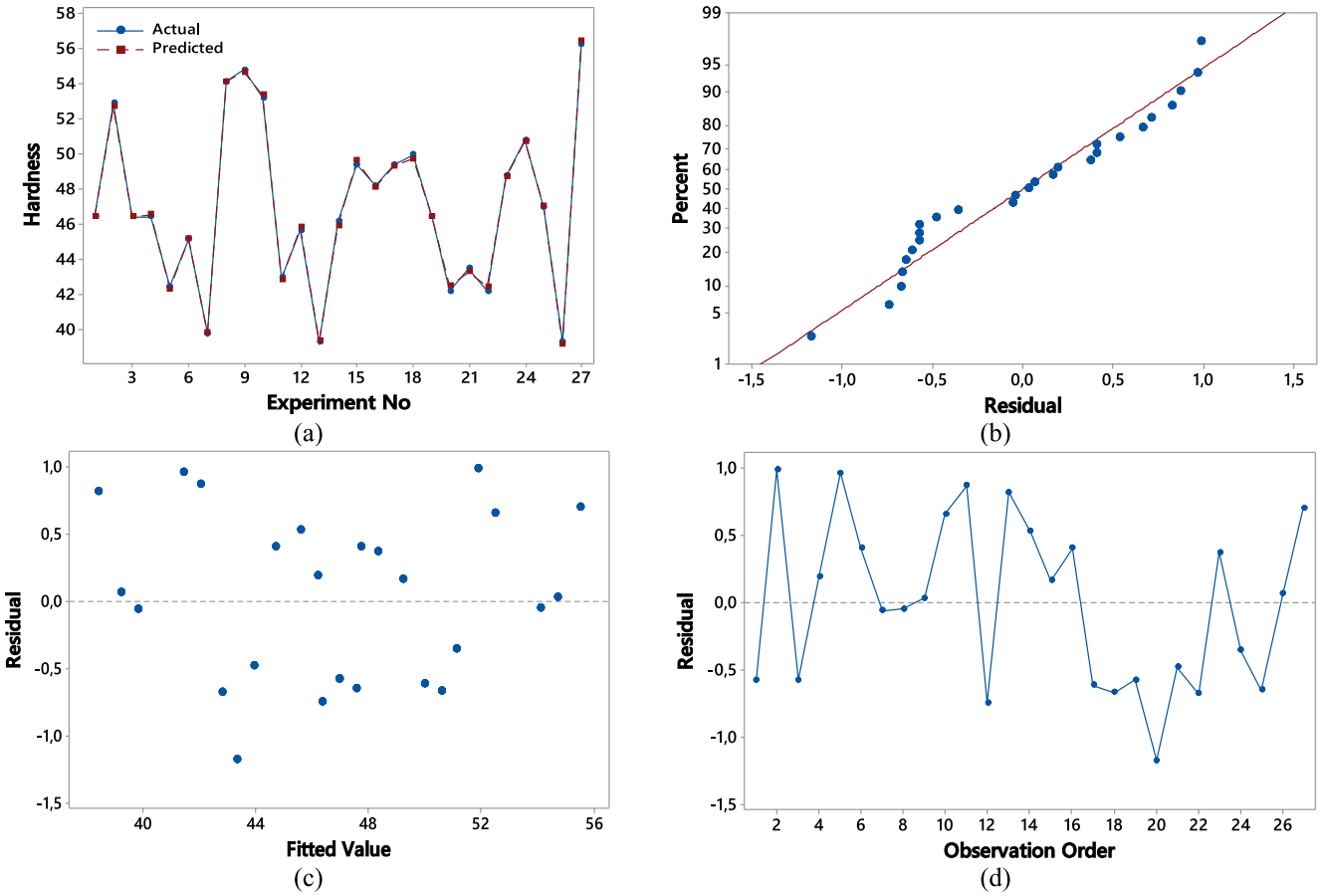

FIGURE 8 | The graphs obtained from the hardness regression analysis based on BBD are presented below (a) Timescale graph for hardness (actual) and (predicted) (b) Normal probability plot of the residuals (c) Residuals vs. the fitted values (d) Residuals vs. the order of the data.

predictions for these points are not reliable. The distribution of the residuals appears homogeneous, i.e., the existing fluctuations do not show a clear increase or decrease (Figure 9d). This situation suggests that the model does not have a heteroskedastic problem.

Figure 10 shows the residual plot results for the Taguchi. The actual and predicted values generally follow a similar trend (Figure 10a). The lines are close to each other, indicating that the model is generally successful in hardness predictions. The curve (red line) indicates that there is a relationship between the residuals and percentiles (Figure 10b). However, ideally, the residuals would be completely distributed around zero, indicating that further tuning is required to improve the model's accuracy. The plot provides some insights into the model's predictive capacity (Figure 10c). Overall, although the model provides a good fit in some regions, errors in certain predictions indicate that the model needs to be further optimized. Significant fluctuations are observed in the residual values (Figure 10d). For the first five observations, the residuals occasionally jump to positive and negative values. This fluctuation may indicate that the model makes inconsistent predictions for these observations.

The coefficient of determination (R^2) measures the extent to which the model explains the variability in the response data relative to its mean. Ranging from 0% to 100%, an R^2 of 0% indicates that the model fails to account for any variation in the response data, while an R^2 of 100% signifies that the model perfectly explains all variability in the response data. Table 6 summarizes the performance of the aforementioned measure results for methods. Each method provides superiority in different aspects in terms of model adequacy. Taguchi has the highest value with 98.91% in terms of R^2 value, indicating the power to explain the data; in addition, the adjusted R^2 value adjusted by considering the number of explanatory variables of the model is also at the highest level for Taguchi with 97.85%. When the predicted R^2 value indicating the prediction accuracy of the model on new data is examined, the highest rate is obtained with 97.35% in BBD. This situation shows that BBD exhibits better performance in terms of prediction success. DSD offers quite good performance in general model fit. R^2 value of DSD is 98.12% and the adjusted R^2 value is 96.94%, indicating that the model has high power to explain the data and provides a good fit considering the number of explanatory variables. However, the predicted R^2 value is slightly lower than the BBD and Taguchi designs at 95.47%, which shows that DSD lags behind the other designs in terms of prediction accuracy. Taguchi has the highest values in terms of R^2 and adjusted R^2, while the BBD is superior in terms of predicted R^2; DSD exhibits a strong performance in overall fit and offers a good model fit.

10991381, 2025, 6, Downloaded from https://onlinelibrary.wiley.com/doi/10.1002/pat.70230 by Turkey National Provision, Wiley Online Library on [10/11/2025]. See the Terms and Conditions (https://onlinelibrary.wiley.com/terms-and-conditions) on Wiley Online Library for rules of use; OA articles are governed by the applicable Creative Commons License

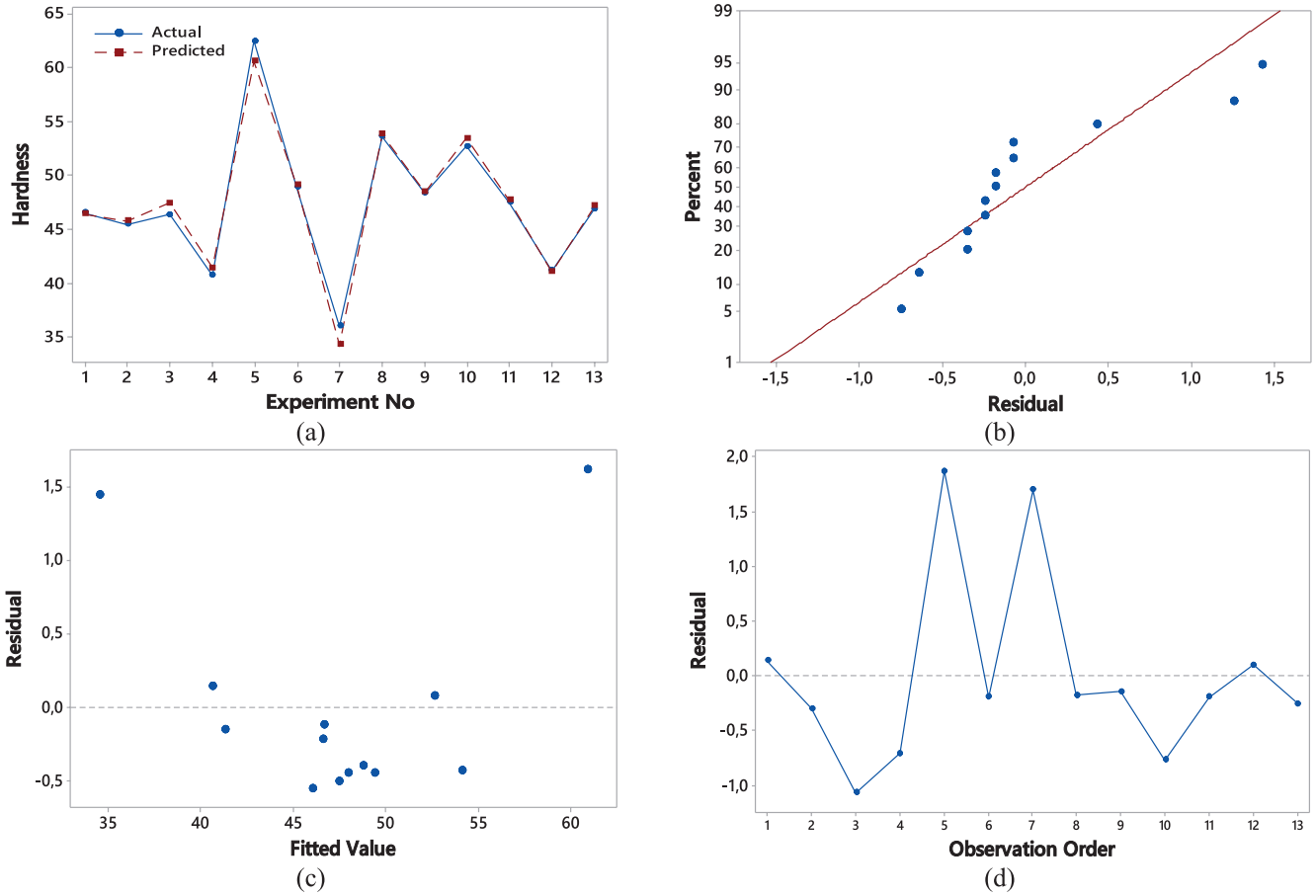

FIGURE 9 | The graphs obtained from the hardness regression analysis based on the DSD are presented below (a) Timescale graph for hardness (actual) and (predicted) (b) Normal probability plot of the residuals (c) Residuals vs. the fitted values (d) Residuals vs. the order of the data.

3.5 | Validation Test

Validation tests were conducted for models generated based on Taguchi, BBD, and DSD to confirm their prediction accuracy. Six experimental studies were conducted outside the original design parameters within the defined levels. The validation test results are summarized in Table 7. The hardness estimation accuracy of each design method varies. Taguchi provided predictions close to the observed values, and the error percentages ranged between 4.51% and 4.98%. The lowest error in Taguchi was observed in test sample number 1 with 4.51%. BBD provided generally lower error percentages, providing an accuracy between 3.24% and 4.08%; the lowest error was seen in test sample number 4 with 3.24%. This result shows that BBD provides more accurate predictions compared to other methods. The DSD provides similar accuracy to Taguchi, with error percentages ranging between 3.88% and 4.72%. DSD achieved the lowest error percentage of 3.88% in test case number 4. The similarity of error percentages shows that DSD outperforms or equals Taguchi in some cases. The BBD showed a better performance in terms of prediction accuracy by standing out with the lowest error percentages. In contrast, the Taguchi and DSD approaches demonstrate marginally lower accuracy than BBD, with comparable levels of prediction error. The actual hardness and predicted hardness for all models are in close agreement, and the error percentage is less than 5% for the six validation tests. Therefore, the prediction accuracy of the generated models is comparable.

3.6 | Optimization

The hardness for both Taguchi, BBD, and DSD is optimized using the desirability function. Table 8 summarizes optimal levels for hardness based on design methods. The table also represents the average values of the desirability function at each level. For each printing factor, the highest value represents the best performance for that level. For instance, among the three levels for ID, the highest value obtained is 0.871, 0.814, and 0.874 at level 1, so it is an optimal level for ID based on the three designs. The optimum levels of the printing factors for three different experimental design methods are given in the table. When interpreting the effects of each design method, the optimal levels determined for each factor can be focused on.

In the design made with the Taguchi, the optimal LT level is 0.628 and this value is at −1 level. The ID and NT reached the values of 0.871 and 0.531, respectively, and were determined as optimal at level 1. In addition, the optimal level of PS is 0.495, which is at −1. In the Taguchi, the PS and LT are focused on lower levels, while the ID and NT are focused on higher levels. In the BBD, the optimal LT value is determined as 0.603 (at 0). The ID is again found at high levels, as 0.814 (at 1), and the NT has a high optimum of 0.508 (at 1). In this design, the PS has a low optimal value of 0.455 (at −1), which indicates that the speed should be reduced. In the design made with the DSD, the optimal level of LT is 0.608, which is at −1. The ID and NT are again selected at

10991581, 2025, 6, Downloaded from https://onlinelibrary.wiley.com/doi/10.1002/pat.70230 by Turkey National Provision, Wiley Online Library on [10/11/2025]. See the Terms and Conditions (https://onlinelibrary.wiley.com/terms-and-conditions) on Wiley Online Library for rules of use; OA articles are governed by the applicable Creative Commons License

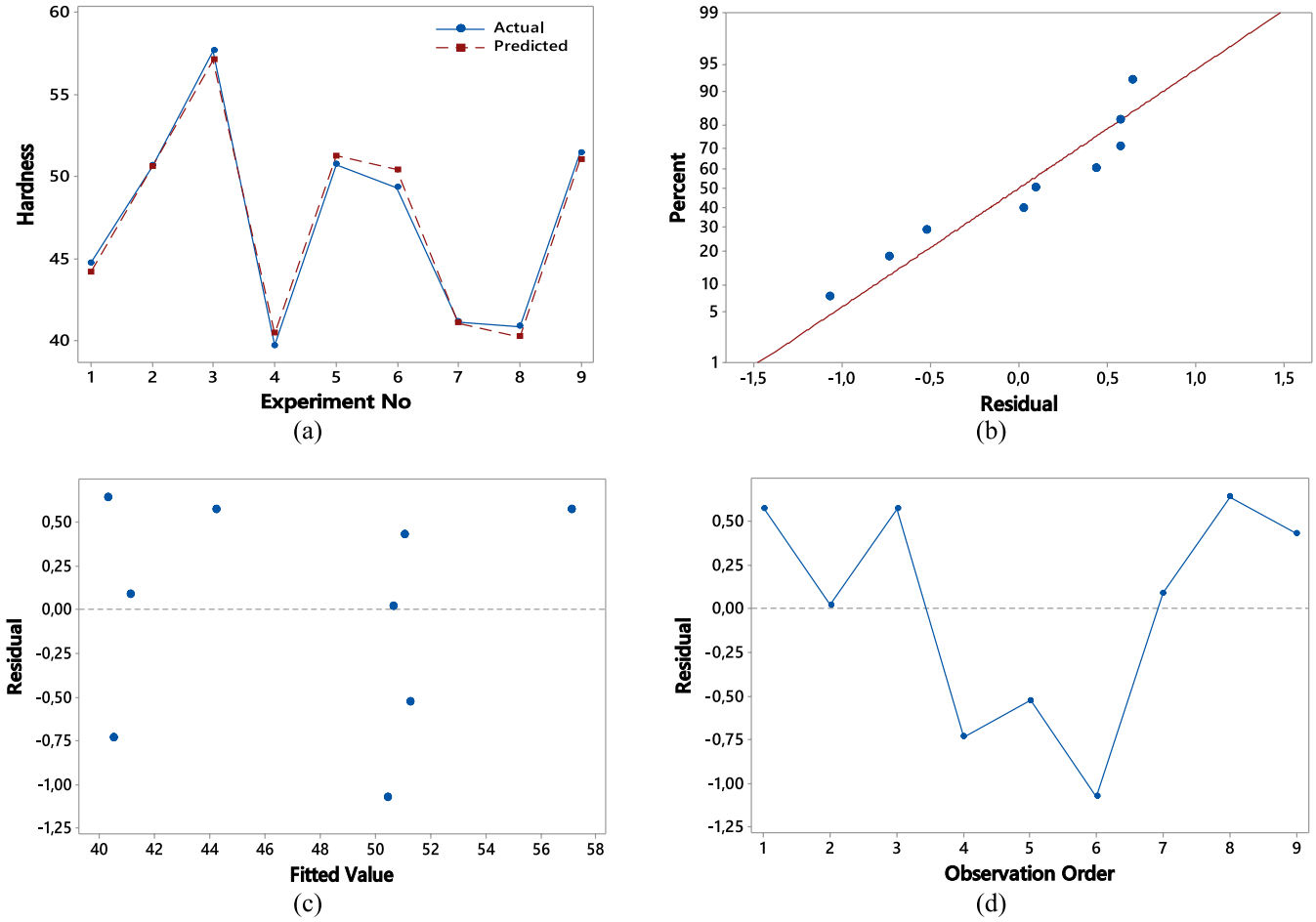

FIGURE 10 | The graphs obtained from the hardness regression analysis based on the Taguchi are presented below (a) Timescale graph for hardness (actual) and (predicted) (b) Normal probability plot of the residuals (c) Residuals vs. the fitted values (d) Residuals vs. the order of the data.

TABLE 6 | Model summary of Taguchi design, BBD, and DSD.

Experimental design	R^2 (%)	Adjusted-R^2 (%)	Predicted-R^2 (%)
Taguchi	98.91	97.85	94.28
BBD	98.27	97.25	97.35
DSD	98.12	96.94	95.47

high levels, as 0.874 and 0.519, respectively. The optimal level of PS is at a medium level, as 0.478 (at 0). In general, different methods revealed that lower levels of LT and PS yield optimal results, while higher levels of ID and NT were more favorable. These results indicate that the PS and LT should be optimized at lower levels, while the ID and NT should be optimized at higher levels.

Finally, confirmation tests were performed to validate the performance of optimal levels (Table 9). In general, there are small

TABLE 7 | Validation test for Taguchi design, BBD, and DSD.

					Surface hardness						
	Printing parameters					Taguchi		BBD		DSD	
No	LT	ID	NT	PS	Actual	Predicted	% Error	Predicted	% Error	Predicted	% Error
1	100	75	240	60	50.21	47.95	4.51	51.98	3.52	52.19	3.94
2	100	100	260	120	59.95	57.03	4.87	62.29	3.91	62.64	4.48
3	200	50	250	90	41.14	43.19	4.98	39.46	4.08	39.25	4.59
4	200	75	240	90	43.71	41.62	4.78	42.29	3.24	45.41	3.88
5	300	100	260	60	54.28	56.98	4.97	56.31	3.73	52.01	4.18
6	300	50	250	120	37.91	36.03	4.95	36.39	4.01	36.12	4.72

10991381, 2025, 6, Downloaded from https://onlinelibrary.wiley.com/doi/10.1002/pat.70230 by Turkey National Provision, Wiley Online Library on [10/11/2025]. See the Terms and Conditions (https://onlinelibrary.wiley.com/terms-and-conditions) on Wiley Online Library for rules of use; OA articles are governed by the applicable Creative Commons License

differences between the predicted and actual hardness, and the percentage error rates are below 5% for all three designs. This shows that all three design methods provide quite accurate results in hardness estimation. The BBD has the lowest error rate, while the DSD and Taguchi methods provide similarly accurate results.

3.7 | Discussion

The comparative analysis of BBD, DSD, and Taguchi methods revealed distinct advantages and limitations for each approach in optimizing PETG part hardness. The BBD demonstrated superior prediction accuracy (3.74% error) but required more experimental runs (27), making it most suitable for applications where precision takes precedence over experimental efficiency. In contrast, the Taguchi method, while showing slightly lower accuracy (4.84% error), required only 9 experimental runs, offering an efficient solution for rapid prototyping and initial parameter optimization. The DSD method provided a balanced compromise with 13 runs and 4.25% errors, making it particularly valuable for industrial applications requiring both reasonable accuracy and experimental efficiency. These findings align with previous research by Gao et al. [51], who reported similar trends in accuracy–efficiency trade-offs, though their study focused on PLA materials. Our results extend these insights specifically to PETG materials, providing new benchmarks for process optimization in this increasingly important polymer.

The consistent identification of ID as the dominant factor across all three methods (contributing 58%–60% to hardness variation) provides robust validation of its critical role in determining PETG part hardness. This finding expands upon Valvez et al.'s [52] work, which identified similar trends but did not quantify the relative contributions of different parameters. The inverse relationship between LT and hardness, particularly pronounced at higher infill densities, suggests a complex interaction that warrants further investigation. The validation tests revealed that while all three methods provided acceptable accuracy, their application requires careful consideration of specific industrial needs. BBD's higher accuracy comes with increased resource requirements, suggesting its use might be most appropriate in high-value applications where precision is critical. The Taguchi method's efficiency makes it particularly suitable for initial parameter optimization and rapid prototyping scenarios. Our results have several practical implications for industrial applications. For high-precision components, BBD is recommended despite higher experimental costs, while the Taguchi method offers efficient parameter optimization for rapid prototyping, and DSD provides an effective compromise for balanced applications. The primary focus should be on infill density optimization, with secondary adjustments to layer thickness and nozzle temperature, while printing speed has minimal impact and can be optimized for productivity. While this study provides comprehensive insights, several limitations should be acknowledged, including material specificity to PETG, unaccounted environmental factors, and unexamined long-term performance characteristics.

The findings of this study have significant implications for various industrial applications. The optimized FDM parameters can be directly implemented in manufacturing settings where PETG components are critical. For instance, in medical device manufacturing, the enhanced surface hardness achieved through these optimized parameters can improve the durability

TABLE 8 | Optimal levels for hardness based on Taguchi design, BBD, and DSD.

Design method	Printing factors	Levels			Optimal levels
		−1	0	1	
Taguchi	Layer thickness	0.628	0.347	0.285	−1
	Infill density	0.325	0.523	0.871	1
	Nozzle temperature	0.247	0.436	0.531	1
	Printing speed	0.495	0.374	0.217	−1
BBD	Layer thickness	0.317	0.603	0.378	0
	Infill density	0.325	0.495	0.814	1
	Nozzle temperature	0.226	0.417	0.508	1
	Printing speed	0.455	0.334	0.207	−1
DSD	Layer thickness	0.608	0.324	0.263	−1
	Infill density	0.305	0.485	0.874	1
	Nozzle temperature	0.236	0.428	0.519	1
	Printing speed	0.227	0.478	0.295	0

TABLE 9 | Validation test for optimal levels in Taguchi design, BBD, and DSD.

	Printig parameters				Hardness		
Design method	LT	ID	NT	PS	Actual	Predicted	% Error
Taguchi	100	100	260	60	62.47	59.68	4.46
BBD	200	100	260	60	57.16	55.16	3.49
DSD	100	100	260	90	59.95	57.49	4.11

10991581, 2025, 6, Downloaded from https://onlinelibrary.wiley.com/doi/10.1002/pat.70230 by Turkey National Provision, Wiley Online Library on [10/11/2025]. See the Terms and Conditions (https://onlinelibrary.wiley.com/terms-and-conditions) on Wiley Online Library for rules of use; OA articles are governed by the applicable Creative Commons License

and performance of patient-specific devices and surgical guides. In automotive applications, these parameters can be applied to produce more robust prototype parts and end-use components with consistent mechanical properties. The developed prediction models also offer practical benefits for quality control processes, allowing manufacturers to predict and maintain consistent hardness values while minimizing material waste and production time. Additionally, consumer product manufacturers can utilize these parameters to improve the durability of PETG printed parts in everyday products. The economic advantage of using Taguchi design compared to BBD is particularly relevant for small to medium-sized manufacturers, offering significant cost and time savings while maintaining acceptable accuracy levels. Future research opportunities include investigation of additional parameters such as print orientation and cooling strategies, integration of advanced techniques like machine learning for parameter optimization and real-time monitoring systems, and extended performance studies focusing on long-term durability and environmental stress resistance. This research contributes to the growing body of knowledge on additive manufacturing optimization, particularly in the context of PETG materials, providing manufacturers with practical guidelines for selecting the most appropriate optimization strategy based on their specific requirements for accuracy, efficiency, and resource allocation.

4 | Conclusions

This study evaluated three experimental design methods—BBD, DSD, and Taguchi—for optimizing surface hardness of PETG parts in FDM printing. The Taguchi design proved most efficient with nine experimental runs, while BBD required 27 runs but achieved the highest prediction accuracy (3.49% error). DSD offered a balanced compromise with 13 runs and 4.11% error. All methods demonstrated robust prediction capabilities with high coefficients of determination ($R^2 > 98\%$) and validation accuracy within 5% error. ID emerged as the primary factor affecting hardness across all methods, followed by LT. The optimal printing parameters were determined for each method, consistently indicating "100%" ID and "260°C" NT as crucial settings. These findings provide manufacturers with practical guidelines for selecting appropriate experimental design methods based on their specific requirements for accuracy versus experimental efficiency. The developed prediction models offer valuable insights for quality control in industrial applications, contributing to the broader understanding of parameter optimization in FDM printing technology.

Ethics Statement

The authors have nothing to report.

Conflicts of Interest

The authors declare no conflicts of interest.

Data Availability Statement

Data sharing not applicable to this article as no datasets were generated or analysed during the current study.

References

1. S. L. Sing, C. F. Tey, J. H. K. Tan, S. Huang, and W. Y. Yeong, "3D Printing of Metals in Rapid Prototyping of Biomaterials: Techniques in Additive Manufacturing," in *Rapid Prototyping of Biomaterials* (Elsevier, 2020), 17–40.

2. A. Al Rashid, S. A. Khan, G. Al-Ghamdi, and M. Koç, "Additive Manufacturing: Technology, Applications, Markets, and Opportunities for the Built Environment," *Automation in Construction* 118 (2020): 103268, https://doi.org/10.1016/j.autcon.2020.103268.

3. M. Khorasani, A. Ghasemi, B. Rolfe, and I. Gibson, "Additive Manufacturing a Powerful Tool for the Aerospace Industry," *Rapid Prototyping Journal* 28 (2022): 87–100, https://doi.org/10.1108/RPJ-01-2021-0009.

4. H. K. Banga, P. Kalra, R. M. Belokar, and R. Kumar, "Customized Design and Additive Manufacturing of Kids' Ankle Foot Orthosis," *Rapid Prototyping Journal* 26 (2020): 1677–1685, https://doi.org/10.1108/RPJ-07-2019-0194.

5. M. Vido, G. C. de Oliveira Neto, S. R. Lourenço, M. Amorim, and M. J. F. Rodrigues, "Computer-Aided Design and Additive Manufacturing for Automotive Prototypes: A Review," *Applied Sciences* 14 (2024): 7155, https://doi.org/10.3390/app14167155.

6. A. Oleff, B. Küster, M. Stonis, and L. Overmeyer, "Process Monitoring for Material Extrusion Additive Manufacturing: A State-Of-The-Art Review," *Progress in Additive Manufacturing* 6 (2021): 705–730, https://doi.org/10.1007/s40964-021-00192-4.

7. K. Rajan, M. Samykano, K. Kadirgama, W. S. W. Harun, and M. M. Rahman, "Fused Deposition Modeling: Process, Materials, Parameters, Properties, and Applications," *International Journal of Advanced Manufacturing Technology* 120 (2022): 1531–1570, https://doi.org/10.1007/s00170-022-08860-7.

8. P. K. Penumakala, J. Santo, and A. Thomas, "A Critical Review on the Fused Deposition Modeling of Thermoplastic Polymer Composites," *Composites. Part B, Engineering* 201 (2020): 108336, https://doi.org/10.1016/j.compositesb.2020.108336.

9. S. Radmanesh, S. Shabangiz, N. Koupaei, and S. A. Hassanzadeh-Tabrizi, "3D Printed Bio Polymeric Materials as a New Perspective for Wound Dressing and Skin Tissue Engineering Applications: A Review," *Journal of Polymer Research* 29 (2022): 50, https://doi.org/10.1007/s10965-022-02899-6.

10. C. V. Subbarao, Y. Srinivasa Reddy, V. Inturi, and M. Indra Reddy, "Dynamic Mechanical Analysis of 3D Printed PETG Material," *IOP Conference Series: Materials Science and Engineering* 1057 (2021): 012031, https://doi.org/10.1088/1757-899X/1057/1/012031.

11. M. El Mehtedi, P. Buonadonna, R. El Mohtadi, G. Loi, F. Aymerich, and M. Carta, "Optimizing Milling Parameters for Enhanced Machinability of 3D-Printed Materials: An Analysis of PLA, PETG, and Carbon-Fiber-Reinforced PETG," *Journal Of Manufacturing And Materials Processing* 8 (2024): 131, https://doi.org/10.3390/jmmp8040131.

12. M. M. Hanon, J. Dobos, and L. Zsidai, "The Influence of 3D Printing Process Parameters on the Mechanical Performance of PLA Polymer and Its Correlation With Hardness," *Procedia Manufacturing* 54 (2021): 244–249, https://doi.org/10.1016/j.promfg.2021.07.038.

13. B. Tyagi, A. Raj, A. Sahai, and R. S. Sharma, "Enhancing Compressive Strength in Polymer Composites Utilized for Application of Foot Prostheses," *Journal of Polymer Research* 31 (2024): 30, https://doi.org/10.1007/s10965-024-03880-1.

14. W. F. Gemechu, W. Sitek, and G. F. Batalha, "Improving Hardenability Modeling: A Bayesian Optimization Approach to Tuning Hyperparameters for Neural Network Regression," *Applied Sciences* 14 (2024): 2554, https://doi.org/10.3390/app14062554.

15. L. A. Román-Ramírez and J. Marco, "Design of Experiments Applied to Lithium-Ion Batteries: A Literature Review," *Applied Energy* 320 (2022): 119305, https://doi.org/10.1016/j.apenergy.2022.119305.

10991381, 2025, 6, Downloaded from https://onlinelibrary.wiley.com/doi/10.1002/pat.70230 by Turkey National Provision, Wiley Online Library on [10/11/2025]. See the Terms and Conditions (https://onlinelibrary.wiley.com/terms-and-conditions) on Wiley Online Library for rules of use; OA articles are governed by the applicable Creative Commons License

16. J. A. Silva, F. M. Braga, F. G. Fermoso, et al., "Evaluation of the Influence of Trace Metals on Methane Production From Domestic Sewage, Using the Plackett-Burman Experimental Design," *Journal of Environmental Management* 294 (2021): 113002, https://doi.org/10.1016/j.jenvman.2021.113002.

17. Y. Du, P. Huang, W. Jin, et al., "Optimization of Extraction or Purification Process of Multiple Components From Natural Products: Entropy Weight Method Combined With Plackett–Burman Design and Central Composite Design," *Molecules* 26, no. 18 (2021): 5572, https://doi.org/10.3390/molecules26185572.

18. S. Oza, P. Kodgire, and S. S. Kachhwaha, "Analysis of RSM Based BBD and CCD Techniques Applied for Biodiesel Production From Waste Cotton-Seed Cooking Oil via Ultrasound Method," *Analytical Chemistry Letters* 12 (2022): 86–101, https://doi.org/10.1080/22297928.2021.2019611.

19. V. Gvoic, M. Prica, M. Turk Sekulic, et al., "Synergistic Effect of Fenton Oxidation and Adsorption Process in Treatment of Azo Printing Dye: DSD Optimization and Reaction Mechanism Interpretation," *Environmental Technology* 45 (2024): 1781–1800, https://doi.org/10.1080/09593330.2022.2154082.

20. K. Rashed, A. Kafi, R. Simons, and S. Bateman, "Fused Filament Fabrication of Nylon 6/66 Copolymer: Parametric Study Comparing Full Factorial and Taguchi Design of Experiments," *Rapid Prototyping Journal* 28 (2022): 1111–1128, https://doi.org/10.1108/RPJ-06-2021-0139.

21. E. Altas, S. Bati, S. Rajendrachari, Ö. Erkan, I. E. Dag, and B. Avar, "Comprehensive Analysis of Mechanical Properties, Wear, and Corrosion Behavior of AA7075-T6 Alloy Subjected to Cryogenic Treatment for Aviation and Defense Applications," *Surface and Coatings Technology* 490 (2024): 131101, https://doi.org/10.1016/j.surfcoat.2024.131101.

22. I. Tamașag, I. Beșliu-Băncescu, T.-L. Severin, C. Dulucheanu, and D.-A. Cerlincă, "Experimental Study of in-Process Heat Treatment on the Mechanical Properties of 3D Printed Thermoplastic Polymer PLA," *Polymers* 15, no. 2367 (2023): 2367, https://doi.org/10.3390/polym15102367.

23. A. I. Portoacă, R. G. Ripeanu, A. Diniță, and M. Tănase, "Optimization of 3D Printing Parameters for Enhanced Surface Quality and Wear Resistance," *Polymers* 15 (2023): 3419, https://doi.org/10.3390/polym15163419.

24. D. Veeman, S. Sudharsan, G. J. Surendhar, R. Shanmugam, and L. Guo, "Machine Learning Model for Predicting the Hardness of Additively Manufactured Acrylonitrile Butadiene Styrene," *Materials Today Communications* 35 (2023): 106147, https://doi.org/10.1016/j.mtcomm.2023.106147.

25. R. Venkatraman and S. Raghuraman, "Experimental Analysis on Density, Micro-Hardness, Surface Roughness and Processing Time of Acrylonitrile Butadiene Styrene (ABS) Through Fused Deposition Modeling (FDM) Using Box Behnken Design (BBD)," *Materials Today Communications* 27 (2021): 102353, https://doi.org/10.1016/j.mtcomm.2021.102353.

26. J. Borah and M. Chandrasekaran, "Predictive Modeling and Optimization of Rockwell Hardness of Additively Manufactured PEEK Using RSM, ANFIS and RNN Integrated With PSO," *Physica Scripta* 99 (2024): 086006, https://doi.org/10.1088/1402-4896/ad6514.

27. M.-H. Hsueh, C.-J. Lai, K.-Y. Liu, et al., "Effects of Printing Temperature and Filling Percentage on the Mechanical Behavior of Fused Deposition Molding Technology Components for 3D Printing," *Polymers* 13, no. 17 (2021): 2910, https://doi.org/10.3390/polym13172910.

28. M. Ajay Kumar, M. S. Khan, and S. B. Mishra, "Effect of Machine Parameters on Strength and Hardness of FDM Printed Carbon Fiber Reinforced PETG Thermoplastics," *Materials Today Proceedings* 27 (2020): 975–983, https://doi.org/10.1016/j.matpr.2020.01.291.

29. M. Kuntoğlu, A. Aslan, H. Sağlam, D. Y. Pimenov, K. Giasin, and T. Mikolajczyk, "Optimization and Analysis of Surface Roughness, Flank Wear and 5 Different Sensorial Data via Tool Condition Monitoring System in Turning of AISI 5140," *Sensors* 20 (2020): 4377, https://doi.org/10.3390/s20164377.

30. D. Y. Pimenov, A. Bustillo, S. Wojciechowski, V. S. Sharma, M. K. Gupta, and M. Kuntoğlu, "Artificial Intelligence Systems for Tool Condition Monitoring in Machining: Analysis and Critical Review," *Journal of Intelligent Manufacturing* 34 (2023): 2079–2121, https://doi.org/10.1007/s10845-022-01923-2.

31. Y. Liu, L. Guo, H. Gao, Z. You, Y. Ye, and B. Zhang, "Machine Vision Based Condition Monitoring and Fault Diagnosis of Machine Tools Using Information From Machined Surface Texture: A Review," *Mechanical Systems and Signal Processing* 164 (2022): 108068, https://doi.org/10.1016/j.ymssp.2021.108068.

32. J. Kumar, V. Mishra, A. Kumar, and S. Negi, "Characterization of 3D Printable Polyethylene Terephthalate Glycol Composite Filament Reinforced With Agricultural Waste Derived From Pineapple Plant," *Journal of Reinforced Plastics and Composites* (2024), https://doi.org/10.1177/07316844241263897.

33. O. Ulkir and G. Akgun, "Prediction of Flexural Strength With Fuzzy Logic Approach for Fused Deposition Modeling of Polyethylene Terephthalate Glycol Components," *Journal of Materials Engineering and Performance* 33 (2024): 4367–4376, https://doi.org/10.1007/s11665-024-09291-z.

34. P. Q. K. Nguyen, J. Panta, T. Famakinwa, et al., "Influences of Printing Parameters on Mechanical Properties of Recycled PET and PETG Using Fused Granular Fabrication Technique," *Polymer Testing* 132 (2024): 108390, https://doi.org/10.1016/j.polymertesting.2024.108390.

35. C. Yan, C. Kleiner, A. Tabigue, et al., "PETG: Applications in Modern Medicine," *Engineered Regeneration* 5 (2024): 45–55, https://doi.org/10.1016/j.engreg.2023.11.001.

36. S. J. A. Ali, D. Rahmatabadi, M. Baghani, and M. Baniassadi, "Design, Processing, 3D/4D Printing, and Characterization of the Novel PETG–PBAT Blends," *Journal of Materials Science* 59 (2024): 9150–9164, https://doi.org/10.1007/s10853-024-09761-8.

37. M. Lalegani Dezaki, M. K. A. Mohd Ariffin, and S. Hatami, "An Overview of Fused Deposition Modelling (FDM): Research, Development and Process Optimisation," *Rapid Prototyping Journal* 27 (2021): 562–582, https://doi.org/10.1108/RPJ-08-2019-0230.

38. A. Sola, W. J. Chong, D. Pejak Simunec, et al., "Open Challenges in Tensile Testing of Additively Manufactured Polymers: A Literature Survey and a Case Study in Fused Filament Fabrication," *Polymer Testing* 117 (2023): 107859, https://doi.org/10.1016/j.polymertesting.2022.107859.

39. S. Vyavahare, S. Teraiya, D. Panghal, and S. Kumar, "Fused Deposition Modelling: A Review," *Rapid Prototyping Journal* 26 (2020): 176–201, https://doi.org/10.1108/RPJ-04-2019-0106.

40. N. Zhang, P. Bénard, R. Chahine, T. Yang, and J. Xiao, "Optimization of Pressure Swing Adsorption for Hydrogen Purification Based on Box-Behnken Design Method," *International Journal of Hydrogen Energy* 46 (2021): 5403–5417, https://doi.org/10.1016/j.ijhydene.2020.11.045.

41. S. Yaghoubi, F. Rabiei, and M. Seidi, "A Comprehensive Assessment on Surface Quality of Machined Wooden Products via Box-Behnken Design Method," *Wood Material Science & Engineering* 19 (2024): 896–905, https://doi.org/10.1080/17480272.2023.2290212.

42. A. Jankovic, G. Chaudhary, and F. Goia, "Designing the Design of Experiments (DOE) – An Investigation on the Influence of Different Factorial Designs on the Characterization of Complex Systems," *Energy and Buildings* 250 (2021): 111298, https://doi.org/10.1016/j.enbuild.2021.111298.

43. M. K. A. Khan, A. S. Abdulhameed, H. Alshahrani, and S. Algburi, "Development of Chitosan Biopolymer by Chemically Modified Orange Peel for Safranin O Dye Removal: A Sustainable Adsorbent and Adsorption Modeling Using RSM-BBD," *International Journal of Biological*

10991581, 2025, 6, Downloaded from https://onlinelibrary.wiley.com/doi/10.1002/pat.70230 by Turkey National Provision, Wiley Online Library on [10/11/2025]. See the Terms and Conditions (https://onlinelibrary.wiley.com/terms-and-conditions) on Wiley Online Library for rules of use; OA articles are governed by the applicable Creative Commons License

Macromolecules 261 (2024): 129964, https://doi.org/10.1016/j.ijbiomac.2024.129964.

44. Y. Bai, Z. Wang, G. Chen, H. Zhou, and W. Zhou, "Enhancing Early-Stage Cell Culture Process Development Efficiency Using an Integrated Approach of High-Throughput Miniaturized Bioreactors and Definitive Screening Design," *Biochemical Engineering Journal* 203 (2024): 109217, https://doi.org/10.1016/j.bej.2024.109217.

45. M. Abas, T. Habib, S. Noor, and K. M. Khan, "Comparative Study of I-Optimal Design and Definitive Screening Design for Developing Prediction Models and Optimization of Average Surface Roughness of PLA Printed Parts Using Fused Deposition Modeling," *International Journal of Advanced Manufacturing Technology* 125 (2023): 689–700, https://doi.org/10.1007/s00170-022-10784-1.

46. H. Favre and A. Chaves Neto, "An Application of Definitive Screening Designs (DSDs) to a Food Product Optimization and Adaptations to Jones & Nachtsheim Methodology for Fitting DSD Models," *Food Quality and Preference* 88 (2021): 104106, https://doi.org/10.1016/j.foodqual.2020.104106.

47. W.-H. Chen, M. Carrera Uribe, E. E. Kwon, et al., "A Comprehensive Review of Thermoelectric Generation Optimization by Statistical Approach: Taguchi Method, Analysis of Variance (ANOVA), and Response Surface Methodology (RSM)," *Renewable and Sustainable Energy Reviews* 169 (2022): 112917, https://doi.org/10.1016/j.rser.2022.112917.

48. J. Wu, Z. Jiang, L. Wan, H. Song, and K. Abbass, "Robust Optimization for Precision Product Using Taguchi-RSM and Desirability Function," *Arabian Journal for Science and Engineering* 46 (2021): 2803–2814, https://doi.org/10.1007/s13369-020-05326-4.

49. N. Almansoori, S. Aldulaijan, S. Althani, N. M. Hassan, M. Ndiaye, and M. Awad, "Manual Spray Painting Process Optimization Using Taguchi Robust Design," *International Journal of Quality & Reliability Management* 38 (2020): 46–67, https://doi.org/10.1108/IJQRM-07-2019-0248.

50. M. Chandna, B. K. Umrao, M. Grover, et al., "Artificial Intelligence in Banking: Regression Analysis for Credit Risk Prediction," in *2025 nternational Conference on Automation and Computation (AUTOCOM)* (IEEE, 2025), 899–904.

51. G. Gao, F. Xu, and J. Xu, "Parametric Optimization of FDM Process for Improving Mechanical Strengths Using Taguchi Method and Response Surface Method: A Comparative Investigation," *Machines* 10 (2022): 750, https://doi.org/10.3390/machines10090750.

52. S. Valvez, A. P. Silva, and P. N. B. Reis, "Optimization of Printing Parameters to Maximize the Mechanical Properties of 3D-Printed PETG-Based Parts," *Polymers* 14, no. 13 (2022): 2564, https://doi.org/10.3390/polym14132564.

10991581, 2025, 6, Downloaded from https://onlinelibrary.wiley.com/doi/10.1002/pat.70230 by Turkey National Provision, Wiley Online Library on [10/11/2025]. See the Terms and Conditions (https://onlinelibrary.wiley.com/terms-and-conditions) on Wiley Online Library for rules of use; OA articles are governed by the applicable Creative Commons License